Chemical and Electrochemical Oxidation of Silicon Surfaces Functionalized with APTES: The Role of Surface Roughness in the AuNPs Anchoring Kinetics

ARTICLE *in* THE JOURNAL OF PHYSICAL CHEMISTRY C · MAY 2013

Impact Factor: 4.77 · DOI: 10.1021/jp212613f

4 AUTHORS, INCLUDING:

Luis A. Pérez
National University of Cordoba, Argentina
14 PUBLICATIONS **69** CITATIONS
SEE PROFILE

Eduardo Andres Coronado
National University of Cordoba, Argentina
60 PUBLICATIONS **5,332** CITATIONS
SEE PROFILE

THE JOURNAL OF PHYSICAL CHEMISTRY C

Article

pubs.acs.org/JPCC

Chemical and Electrochemical Oxidation of Silicon Surfaces Functionalized with APTES: The Role of Surface Roughness in the AuNPs Anchoring Kinetics

Joaquín Klug, Luis A. Pérez, Eduardo A. Coronado,* and Gabriela I. Lacconi*

INFIQC, Departamento de Fisicoquímica, Facultad de Ciencias Químicas, Universidad Nacional de Córdoba, Haya de la Torre - Medina Allende, Ciudad Universitaria, 5000 Córdoba, Argentina

Supporting Information

ABSTRACT: Oxidation of Si(111) surfaces is a procedure widely used for their further functionalization with 3-aminopropyltriethoxysilane (APTES). In the present work, the formation of silicon oxide is carried out by chemical and electrochemical oxidation of the hydrogenated-silicon surfaces, giving rise to ***Si-Ox***^{Chem} and ***Si-Ox***^{Echem} surfaces, respectively. Both surfaces are then functionalized with APTES solution to form an aminopropylsilane (APS) film, using two quite different concentrations of APTES (0.001 and 0.1% v/v), to compare two limiting situations. At the lowest APTES concentration, the comparison of the kinetics of gold nanoparticles (AuNPs) anchoring process on both surfaces is found to be quite different, not only in the initial rate of NPs anchoring but also in the maximum percentage of coverage. In contrast, the kinetics behavior is almost the same when the surfaces are modified with the highest APTES concentration, reaching the same value of surface coverage. The different or similar behavior of both surfaces is analyzed by a careful characterization of ***Si-Ox***^{Chem} and ***Si-Ox***^{Echem} surfaces using XP spectroscopy and AFM measurements, before and after APS functionalization. The significant differences in the surface roughness of the ***Si-Ox*** samples, together with the determination of the number of $-NH_3^+$ moieties after silanization at both APTES concentrations, leads to the conclusion that the availability of $-NH_3^+$ moieties is dependent on two factors: the roughness of the ***Si-Ox***^{Chem} and ***Si-Ox***^{Echem} surfaces as well as the concentration of the APTES solutions. When the APS layer is formed at the lowest APTES concentration, surface roughness controls the number of different types of nitrogen functional groups. In contrast, at the highest APTES concentration, the surface roughness does not have any significant role in the number of $-NH_3^+$ moieties present on both surfaces. Because the kinetics of AuNPs anchoring depends mainly on the probability of interacting with the $-NH_3^+$ groups, the above characterization allows us to explain in a consistent way the kinetics behavior observed for each particular condition of surface preparation.

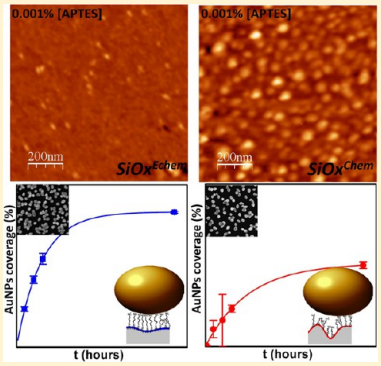

1. INTRODUCTION

Solid platforms containing noble-metal nanoparticles assemblies on the surface are currently the subject of considerable interest due to their potential applications in biosensing, optical, and electronic devices.[1−5] In particular, in recent years many strategies for building robust and controlled supported gold nanoparticles (AuNPs) assemblies on different type of surfaces have been developed.[6−8] The key role played by the NP size, shape, interparticle separation, and the nature of the interaction of these assemblies with the solid substrate is due to the dependence of their physical and chemical properties that can be generated by a subtle change of any of these parameters.[8−10]

Usually, the anchoring of NPs on the solid substrates is carried out by using an intermediate layer of molecular structures on the surface, which gives rise to electrostatic or chemical interactions between NPs and their functional groups. Therefore, the molecules for such intermediate layers have headgroups with adequate functionalities to interact with NPs.[11−13] Ideally, these platforms should be quite stable over time and robust; that is, NPs attached to the surface should be difficult to remove and suitable to be further functionalized if necessary. Despite the great interest in developing new protocols for building these platforms, there are only a few reports that address the fundamental issue of studying the influence of the solid surface characteristics on the NPs "anchoring" capabilities of the substrate despite the well-known fact that the properties of the substrate surface (crystalline structure, chemical characteristics, surface defects, surface roughness, etc.) can substantially modify the NPs adhesion.[14−18]

AuNPs immobilization on glass slide surfaces is a common method to obtain homogeneous NPs assemblies. This procedure is often performed by functionalization with organosilane molecules.[18−23] In particular, the use of 3-aminopropyltriethoxysilane (APTES) for the functionalization of glass slides is one of the most popular procedures for building AuNPs assemblies platforms. The silanization reaction

Received: December 30, 2011
Revised: May 6, 2013
Published: May 8, 2013

dx.doi.org/10.1021/jp212613f | J. Phys. Chem. C 2013, 117, 11317−11327

involves the hydroxylation of glass or silicon oxide surface and the hydrolysis of the APTES ethoxy groups. This procedure yields to an aminopropylsilane (APS) layer having amino-terminal groups on the surface, whose interaction with AuNPs determines the degree of NP surface coverage.[14,17−25]

Although APTES functionalization has been extensively studied, because of the ability of organosilane molecules to polymerize on the surface, the resulting structure and coverage of the layers are highly dependent on several parameters such as temperature,[26] humidity[27−29] (a quantity necessary to catalyze the first step of the reaction), concentration of the APTES solution, immersion time, and so on.

The aim of this work is to study the influence of the oxidation pretreatment (chemical or electrochemical) for generating thin film oxide layers on silicon (Si(111)) surfaces able to be functionalized with APTES on the kinetics of the AuNPs anchoring process. Both surfaces ***Si-Ox^{Echem}*** and ***Si-Ox^{Chem}*** obtained by electrochemical and chemical methods, respectively, were functionalized using two quite different APTES concentrations under the same conditions (solvent, humidity, and temperature). After silanization, an APS layer is expected to be formed on both ***Si-Ox*** surfaces. The kinetics of the AuNPs anchoring process was followed at different time periods (from 6 to 120 h) by determining the degree of AuNPs surface coverage at each time. Significant differences on the kinetics behavior were observed for APS-functionalized ***Si-Ox^{Echem}*** and ***Si-Ox^{Chem}*** surfaces using the lowest APTES concentration. In contrast, the kinetics of AuNPs surface coverage was found to be almost the same for ***Si-Ox^{Echem}*** and ***Si-Ox^{Chem}*** surfaces modified with APTES at the highest concentration. The kinetic behavior observed for each type of substrate was rationalized by characterizing both surfaces before and after APS-functionalization with X-ray photoelectron spectroscopy (XPS) and atomic force microscopy (AFM).

2. EXPERIMENTAL SECTION

2.1. Materials and Methods. Hydrogen tetrachloroaurate ($HAuCl_4{\cdot}3H_20$) and sodium citrate were purchased from Carlo Erba and Anhedra, respectively, and used as received without further purification. APTES was purchased from Sigma-Aldrich. All other chemicals reagents employed in the experiments were of analytical grade. Milli-Q water (18.2 MΩ cm) was used for preparation of solutions.

n-type Si wafers (as-doped and a specific resistivity of 0.001 to 0.005 Ω cm) with (111) orientation from Virginia Semiconductors were used as substrates for further electrochemical or chemical oxidation.

Electrochemical experiments of silicon oxide formation were performed in a standard three-electrode glass cell with a saturated calomel reference and a Pt counter electrode. All potentials are referred to that of the saturated calomel electrode (SCE). Silicon samples were introduced in a Teflon holder exposing a surface area of 0.541 cm^2 and used as working electrodes. In/Ga eutectic was used as the ohmic back contact. Electrochemical measurements were carried out with an Autolab PGSTAT 100 (ECO−CHEMIE) instrument.

XPS of the oxidized and APTES-functionalized silicon substrates was performed using a Mg Kα source at 13 kV and 300 W (XR 50, Specs) and a hemispherical electron energy analyzer (PHOIBOS 100 MCD, Specs) with an electron takeoff angle of 90°. Spectra covering a wide range of energies have been taken from 0 to 1100 eV with 40 eV and the multiregion spectra (narrow energy regions of interest), with 10 eV pass energy. A two-point calibration of the energy scale was performed using sputtered cleaned gold (Au $4f_{7/2}$, binding energy = 84.00 eV) and copper (Cu $2p_{3/2}$, binding energy = 932.67 eV) samples. Spectra were analyzed with CasaXPS v2.3.14 and XPS Peak 4.1 software packages. The fitting of the Si 2p peaks was carried out using a spin−orbit splitting of 0.6 eV and a branching ratio of 0.5. For spectra deconvolution in the N1s and Si2p regions, a Shirley-type background and a Gaussian−Lorentzian function were used.

AFM topographic images of silicon substrates were obtained with a Bruker-Innova AFM system, operated in tapping mode in air. All AFM experiments were conducted under controlled environmental conditions: temperature 20.0 ± 0.3 °C and relative humidity 45 ± 10%. The topographic images were taken with silicon tips (AppNano 20−90 N m^{1-} nominal spring constant) and 145−230 kHz. Image processing and the determination of the roughness (root-mean-square, rms) were performed using WSxM software.[30] The rms value for each surface was calculated considering all the image data in the scanned area on the surface (around 60 000 points).

Extinction spectra of the Au colloidal suspensions were measured with a Shimadzu UV-1601 spectrophotometer, and TEM images of AuNPs were obtained with a JEM-Jeol 1120 electron microscope, employing an 80 kV accelerating voltage. Samples were prepared by depositing a drop of the colloidal solution on a Formvar-carbon-coated copper grid and dried at room temperature.

Images of NPs film on the different substrates were taken by a field-emission scanning electron microscope (FE-SEM) (Zeiss, ΣIGMA). FE-SEM observations were carried out at 10−20 kV.

2.2. Silicon Surface Treatments. *Preparation of Hydrogenated Silicon Surface, **Si-H**.* Si(111) surfaces were first sonicated in ethanol for 5 min and rinsed with milli-Q water. The clean samples were immersed in 1:20 (v/v) HF aqueous solution for 30 s to eliminate the native oxide formed on the surface and rinsed with milli-Q water. Hydrogenation of the surface was performed by immersion in oxygen-free 40% NH_4F solution for 3 min. Finally, the samples were rinsed with water, sonicated, and dried in ultrapure nitrogen stream.

*Preparation of Electrochemically Oxidized Silicon Surface, **Si-Ox^{Echem}***. A thin oxide layer on the silicon surface was obtained applying a potential pulse to the hydrogenated surfaces from −0.6 to 0.2 V versus SCE in 0.1 M acetate buffer solution at pH 5.5 at room temperature. The anodic pulse was applied for 100 s, which is enough time to pass a charge density of 1.0 mC cm^{-2} able to oxidize only a few layers of silicon surface.[31] Cyclic voltammetry in the anodic potential region (between −0.6 and 1.5 V) at 0.02 V s^{-1} was employed for electrochemical characterization of different silicon surfaces.

*Preparation of Chemically Oxidized Silicon Surface, **Si-Ox^{Chem}***. Freshly hydrogenated-silicon samples were chemically oxidized with a piranha solution (mixture of sulfuric acid and hydrogen peroxide, 3:1 (v/v)) at 80 °C for 60 min. The substrates were thoroughly rinsed with milli-Q water and dried in nitrogen stream. *Caution! Piranha solution reacts violently with organic matter and should be handled with extreme care!*

2.3. Gold NPs Preparation and Characterization. A colloidal solution of AuNPs with a diameter of ∼60 nm was prepared by reducing a 0.0025 M $HAuCl_4$ solution with sodium citrate by Turkevich et al. method.[32] The AuNPs were stabilized by a citrate external layer (negative charge) in the colloidal dispersion. The NPs sizes were determined by TEM

and also by UV−visible spectroscopy. (See Figures S1−S3 in the Supporting Information.)

2.4. Assembly of AuNPs onto the APTES-Functionalized Silicon Substrates. *APTES Functionalization.* APTES films were deposited onto the silicon-oxidized substrates by immersion in 0.001 and 0.1% APTES solutions with anhydrous toluene as the solvent for 30 min at room temperature. Then, the substrates were rinsed with toluene, immersed in anhydrous toluene for 20 min, and sonicated in ethanol and water to eliminate the physiadsorbed molecules.[33]

AuNPs Immobilization. Functionalized samples were immersed in AuNPs colloidal dispersions during different immobilization times and after that rinsed and sonicated with water.

The surface density of the NPs was determined as the fraction of the area occupied by NPs on a representative area of the sample using the SEM images. The processing of the SEM images was performed using ImageJ software by Image Processing and Analysis in Java.

3. RESULTS AND DISCUSSION

3.1. Preparation of *Si-H*, *Si-Ox*^{Echem}, and *Si-Ox*^{Chem} Surfaces. Hydrogenated-Si(111) surfaces prepared with a simple wet-chemical method (See Section 2) were used as the initial solid support to be further oxidized. Hydrogen termination evidently results in a chemical passivation of silicon surfaces.[34] The stability and high hydrophobicity degree of the hydrogen layer formed on the silicon surface ensures a well-defined initial state (highly reproducible) for the oxidation process.[35] ***Si-Ox***^{Echem} and ***Si-Ox***^{Chem} surfaces were prepared by anodic and chemical oxidation of the ***Si-H*** samples, as detailed in Section 2. Characterization of ***Si-H***, ***Si-Ox***^{Echem}, and ***Si-Ox***^{Chem} surfaces was performed through the electrochemical behavior of these electrodes by cyclic voltammetry in acetate aqueous solution (Figure 1). In the voltammograms it is clearly observed that the first anodic oxidation steps of ***Si(111)-H*** electrodes (black curve) are represented by two current peaks at around 0 (peak A_I) and 1.0 V (peak A_{II}). The first maximum (A_I peak) with a charge density around 1.0 mC cm^{-2} corresponds to the oxidation of the topmost silicon atoms with rupture of Si−Si and Si−H bonds.[31,36] This charge density

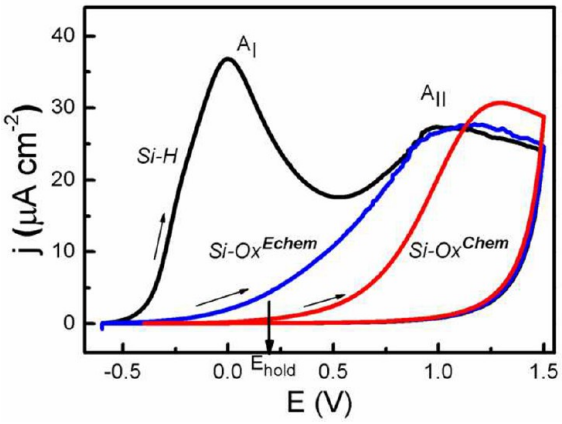

Figure 1. Voltammograms of different silicon electrodes in acetate buffer solution at pH 5.5: ***Si-H*** (black line) and ***Si-Ox***^{Echem} (blue line) after previous anodic oxidation of ***Si-H*** at 0.2 V (E_{hold}) for 100 s and ***Si-Ox***^{Chem} (red line) after chemical oxidation in piranha solution of ***Si-H*** at 80 °C for 60 min. Scan rate: 0.02 V s^{-1}.

is approximately the one calculated for the oxidation of two layers of Si atoms of an ideal Si(111) surface, although in the present case the ***Si-H*** electrodes have certain surface roughness on the atomic scale. (See Section 3.3.)[31] At more positive potentials, the A_{II} peak is attributed to the oxidation of the underlying atom layers; therefore, the thickness of the oxide layer increases.

Because oxide layers formed onto crystalline silicon surfaces are passivating films, it is possible to analyze through cyclic voltammetry the electrochemical growth of the oxide layer on ***Si-Ox***^{Echem} and ***Si-Ox***^{Chem} electrodes. The blue curve in Figure 1 depicts the voltammetric behavior of ***Si-Ox***^{Echem} electrodes immediately after applying the potential pulse at 0.2 V (in slightly acidic solutions, pH 5.5). The current peak A_I is absent in this voltammogram because the topmost silicon atoms have already been oxidized in the previous anodic pulse. Further oxidation proceeds without any additional current peaks. The electrochemical behavior of ***Si-Ox***^{Chem} samples (red curve in Figure 1) is equivalent to that obtained for the ***Si-Ox***^{Echem}, except for the A_{II} peak potential shifting to more positive values. This different electrochemical response could be associated with differences in the oxide thickness or surface roughness of the electrodes, features that are difficult to be determined just by this simple analysis of the voltammograms. An answer to this issue is given in Section 3.3.

3.2. APTES Functionalization of *Si-Ox*^{Chem} **and *Si-Ox***^{Echem} **Surfaces and Kinetics of the AuNPs Anchoring.** The oxidized surfaces are suitable to be functionalized with APTES. As it has been proposed by Chabal and other authors,[14,26,37] a covalent bond between the silanol groups and the APTES molecules occurs after the hydrolysis in aqueous media of the alkoxy groups. Determining in a direct way the surface density of APTES molecules covalently bond to the surface is a very difficult task. However, because the APS layer provides receptor sites for AuNPs, the relative percentage of the above-mentioned sites between different APS layers could, in principle, be estimated by analyzing the number of AuNPs attached to the surface.

In the present work, two limiting conditions of APTES were used to functionalize both types of surfaces (***Si-Ox***^{Chem} and ***Si-Ox***^{Echem}). First, we will present the results obtained after AuNPs immobilization on APS-functionalized ***Si-Ox***^{Chem} and ***Si-Ox***^{Echem} surfaces at the lowest APTES concentration (0.001%). The NPs-area coverage percentage relative to the geometric area of the reference sample was calculated from SEM images. SEM images (Figure 2) clearly show that the NPs surface coverage percentage increases with the immersion time t for both ***Si-Ox***^{Chem} and ***Si-Ox***^{Echem} surfaces. However, comparing the same immersion time, the electrochemical oxidized samples depict a higher degree of surface coverage.

The SEM images sequence at different t for ***Si-Ox***^{Chem} and ***Si-Ox***^{Echem} surfaces after functionalization in concentrated APTES solution (0.1%) is shown in Figure 3. In this case, at variance with the results shown in Figure 2, for the same t, the AuNPs percentage surface coverage for the ***Si-Ox***^{Chem} and ***Si-Ox***^{Echem} surfaces is almost the same. The only significant feature that can be evidenced is that the NPs distribution on ***Si-Ox***^{Echem} surfaces is more homogeneous than that in the ***Si-Ox***^{Chem} surfaces.

In principle, the AuNPs anchoring kinetics can be described according to the following equilibrium:

dx.doi.org/10.1021/jp212613f | J. Phys. Chem. C 2013, 117, 11317−11327

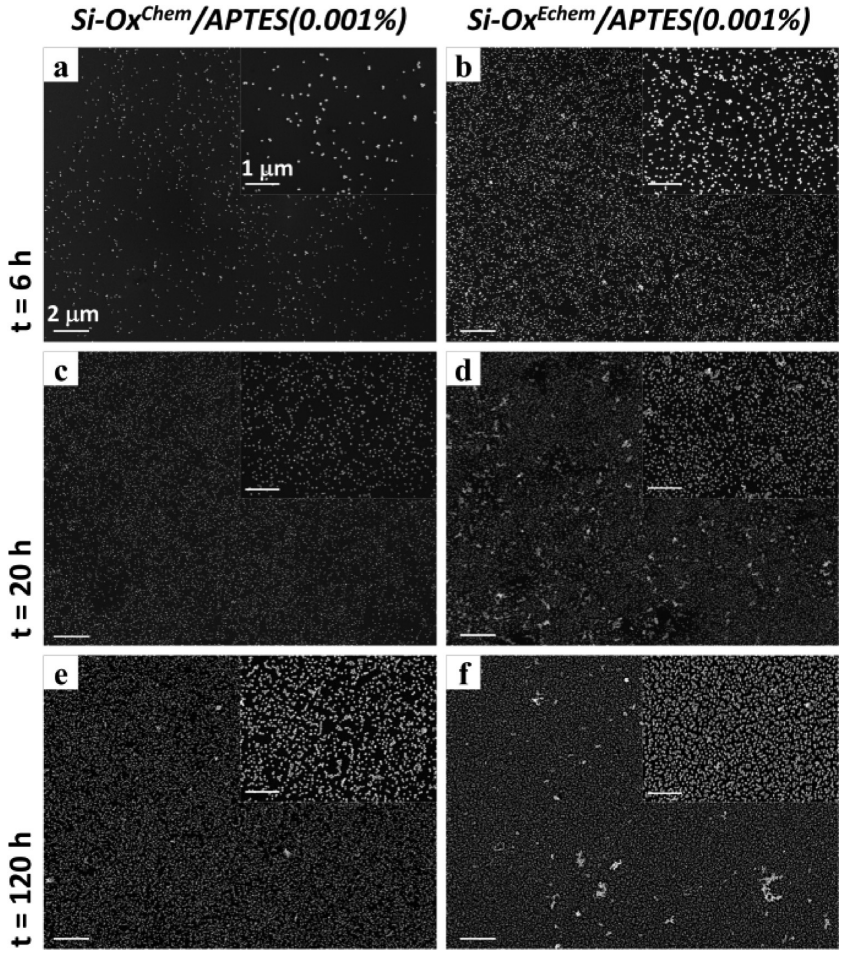

Figure 2. SEM images displaying 60 nm AuNPs deposited on APTES-modified ***Si-Ox***^{Chem} (a,c,e) and ***Si-Ox***^{Echem} (b,d,f) surfaces after an immersion time of $6 \leq t \leq 120$ h in the colloidal solution. APTES concentration in the functionalization bath: 0.001%.

$$S + NP \underset{k_{-1}}{\overset{k_1}{\rightleftarrows}} S_{NP} \tag{1}$$

where S corresponds to the free sites on the APS layer (each site could be formed by several amino-terminal groups), NP corresponds to the gold NPs to be anchored to these sites, and S_{NP} are the sites occupied by AuNPs.

It should be noted that this model for the anchoring kinetics is a simplified one because k_1 may involve several steps such as diffusion of the particle to the site to be anchored, attachment of the NP to the site via electrostatic/chemical interactions, and so on. Therefore, k_1 should be considered as an effective rate constant. In the above kinetic equation, k_{-1} can be regarded as almost negligible because it is highly improbable for a AuNP to leave the surface and therefore the anchoring process can be regarded quasi-irreversible due to the strong interaction between the site and the NP. To probe the irreversibility of AuNPs anchoring process, we have immersed the substrates containing AuNPs for 1 day in water; after that no measurable NP release into the solution was observed (Figure S4, Supporting Information).

Because the number density of NPs in the solution is by far greater than the surface density of sites, it is a very good approximation to consider that the NPs concentration is constant during the experiment. Therefore, the anchoring process follows a pseudo-first-order kinetics,

$$\frac{dS_{NP}(t)}{dt} = \frac{-dS(t)}{dt} = k_1 S(t) \tag{2}$$

Because the total number of sites $S_T = S(t) + S_{NP}(t)$ is constant, replacing $S(t)$ in eq 2 by $S(t) = S_T - S_{NP}(t)$, the following expression is easily obtained after integration:

$$S_{NP}(t) = S_T(1 - e^{-k_1 t}) \tag{3}$$

Multiplying both sides of eq 3 by the footprint area of a single NP, A_{NP}, and dividing by the reference area selected, A_R (in our case 1 μm^2), the area fraction occupied by the NPs can be obtained:

$$f(t) = \frac{A_{NP}S_{NP}}{A_R} = \frac{A_{NP}S_T}{A_R}(1 - e^{-k_1 t}) \tag{4}$$

We are interested indeed in the percentage of NPs surface coverage $\sigma(t) = 100 \times f(t)$; therefore, under the pseudo-first-order kinetics, the evolution of σ with time will be given by:

$$\sigma(t) = \sigma_m(1 - e^{-k_1 t}) \tag{5}$$

where σ_m is the maximum asymptotic value reached as $t \to \infty$.

A quantitative analysis of the AuNPs surface coverage σ was computed by the ratio of geometric area occupied by AuNPs and a representative area of ~25 μm^2 of the sample. This calculation was performed for each experiment choosing different regions on the same sample from the SEM images

dx.doi.org/10.1021/jp212613f | J. Phys. Chem. C 2013, 117, 11317−11327

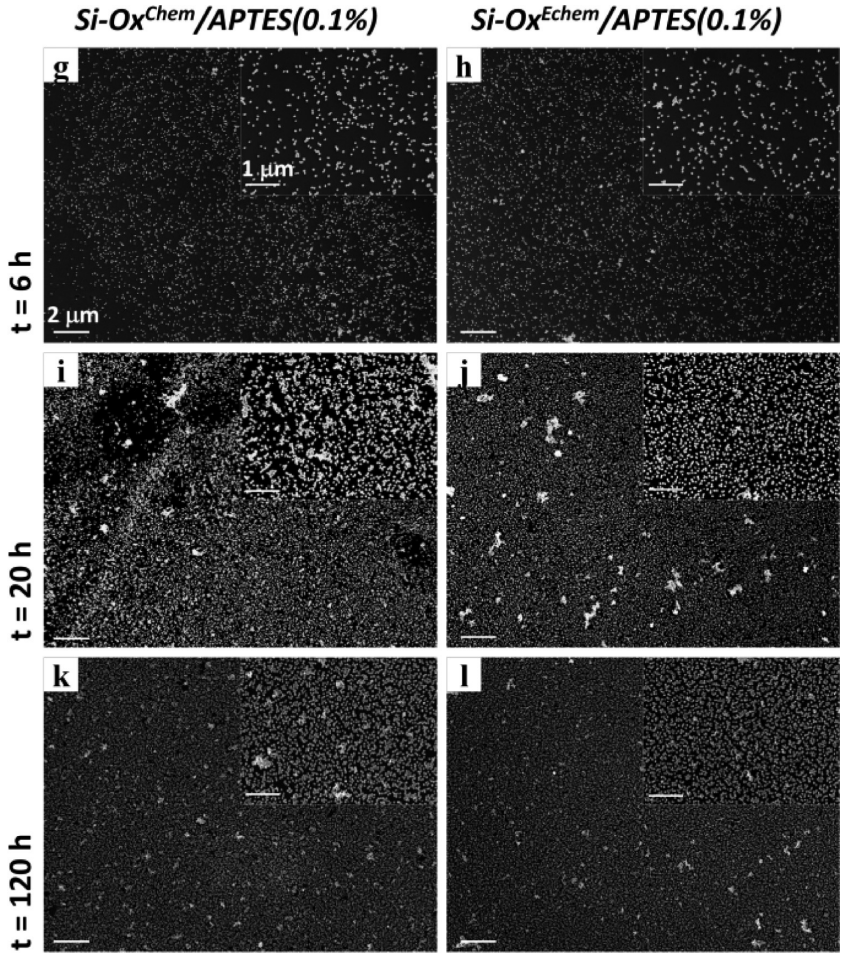

Figure 3. SEM images displaying 60 nm AuNPs deposited on APTES-modified ***Si-Ox***^{Chem} (g,i,k) and ***Si-Ox***^{Echem} (h,j,l) surfaces after immersion times of $6 \leq t \leq 120$ h in the colloidal solution. APTES concentration in the functionalization bath: 0.1%.

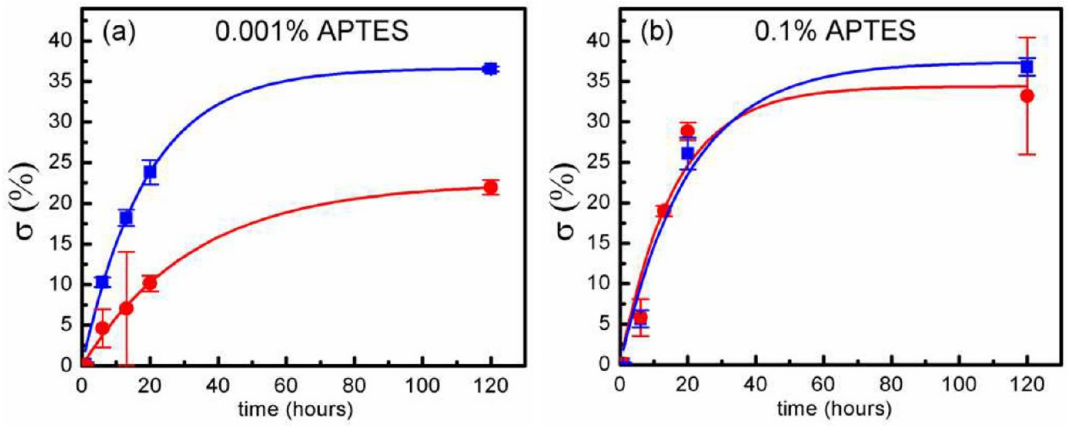

Figure 4. Dependence of the percentage of NPs surface coverage (σ) on the immersion time. σ was calculated from SEM images of Figures 2 and 3 for ***Si-Ox***^{Echem} (blue symbols) and ***Si-Ox***^{Chem} (red symbols) surfaces. Solid lines correspond to the fit of the experimental data with eq 5. Samples were functionalized in 0.001% APTES (a) and 0.1% APTES (b) solutions.

(Figures 2 and 3). The results for both oxidized samples after functionalization with diluted (0.001%) and concentrated (0.1%) APTES solutions, at different t in the colloidal solution, are shown in Figure 4. Independent of the sample, the experimental time dependence of σ follows quite nicely eq 5, corroborating the simple kinetic model approach assumed.

At the lowest APTES concentration the value of σ_m for the ***Si-Ox***^{Echem} surface is ~68% higher than the ***Si-Ox***^{Chem} surface (Figure 4a). This behavior could be explained if the surface density of amino terminal groups on the ***Si-Ox***^{Echem} surface is significantly higher than that on the other surface. In contrast, the $\sigma(t)$ curves shown in Figure 4b for both surfaces are almost the same when the APTES concentration is 0.1%. One explanation of this different behavior could be attributed to the structure of the APS layer.[18,38] Therefore, the different kinetics behavior observed at the lowest APTES concentration

dx.doi.org/10.1021/jp212613f | J. Phys. Chem. C 2013, 117, 11317−11327

Table 1. Kinetics Parameters of AuNPs Anchoring Process on the *Si-Ox*^{Echem} and *Si-Ox*^{Chem} Surfaces Obtained by Fitting the Experimental Data from Figure 4 with Equation 5

	0.001% APTES		0.1% APTES	
	σ_m	k_1 (h^{-1})	σ_m	k_1 (h^{-1})
***Si-Ox*^{Echem}**	(37 ± 1)	(0.053 ± 0.003)	(37 ± 4)	(0.05 ± 0.01)
***Si-Ox*^{Chem}**	(22.5 ± 0.7)	(0.030 ± 0.002)	(34 ± 4)	(0.06 ± 0.02)

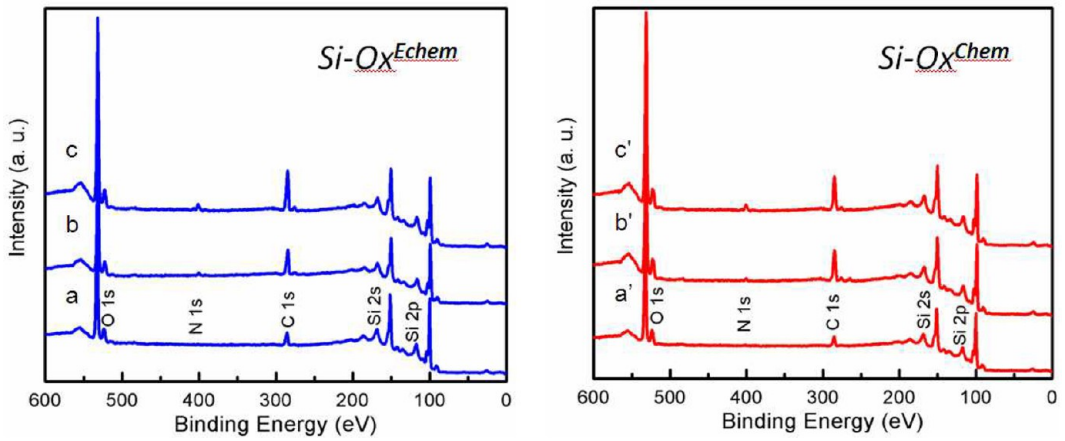

Figure 5. XP spectra for ***Si-Ox*^{Echem}** (blue lines) and ***Si-Ox*^{Chem}** (red lines) surfaces before (a,a′) and after APS functionalization in 0.001% (b,b′) or 0.1% (c,c′) APTES solutions.

Table 2. Normalized Percentage of Amino Species of APS-Functionalized *Si-Ox*^{Echem} and *Si-Ox*^{Chem} Surfaces Determined from N 1s and Si 2p XPS Signals in Figure 6[a]

	***Si-Ox*^{Echem}**		***Si-Ox*^{Chem}**	
N1s/Si2p(0)	0.001% APTES	0.1% APTES	0.001% APTES	0.1% APTES
$-NH_2$	0.9 ± 0.5 (26)	1.9 ± 0.5 (26)	0.9 ± 0.5 (34)	1.6 ± 0.5 (24)
$-NH_3^+$	1.8 ± 0.5 (51)	2.7 ± 0.5 (36)	0.7 ± 0.5 (27)	2.6 ± 0.5 (39)
RNH_2-OSi	0.8 ± 0.5 (23)	2.8 ± 0.5 (38)	1.1 ± 0.5 (39)	2.5 ± 0.5 (37)
N1s total	3.5 ± 0.5(100)	7.4 ± 0.5(100)	2.7 ± 0.5(100)	6.7 ± 0.5(100)
d_{ox} (nm)	1.1 ± 0.1		1.2 ± 0.1	

[a]Values in parentheses correspond to the percentage normalized with respect to the total N 1s content in each column. Oxide thickness calculated from integration of Si 2p XPS signals of both oxidized samples. (See Figure S5 in Supporting Information.)

could, in principle, be explained considering that there is a lower availability of amino groups on the ***Si-Ox*^{Chem}** surface than on the ***Si-Ox*^{Echem}** surface. At the highest APTES concentration, this "availability" should be the same.

The parameters of the optimization of the $\sigma(t)$ curves are shown in Table 1. As discussed above $t \to \infty$, σ_m is ~36% for both APS-functionalized surfaces at the highest APTES concentration. However, at the lowest APTES concentration, σ_m for the ***Si-Ox*^{Echem}** surface is almost similar (37%) to the value reached with concentrated APTES solutions. Besides, σ_m for the ***Si-Ox*^{Chem}** surfaces at the lowest APTES concentration is almost 1.6 times smaller than the electrochemically pretreated surface. Another parameter to be considered that supports this conclusion is the initial rate v_0, which can be obtained by analyzing the kinetics of the AuNPs anchoring at short times (eq 6).

$$v_o = \left(\frac{\partial\sigma}{\partial t}\right)_{t\to 0} = \sigma_m k_1 \tag{6}$$

Equation 6 is obtained by taking the derivative of eq 5 in the limit $t \to 0$. Therefore, at very short times, a linear dependence of σ versus t is expected, as shown in Figure 4. Considering the data from Table 1 for the lowest APTES concentration, the values of v_0 calculated using eq 6 are 2.07 and 0.67 h^{-1} for the ***Si-Ox*^{Echem}** and ***Si-Ox*^{Chem}** surfaces, respectively. The initial rate is around three times faster for the ***Si-Ox*^{Echem}** surface. As a consequence, it should be assumed that the availability of amino groups in the early stages could be by far more important in the electrochemical oxidized surface.

3.3. AFM and XPS Characterization of APS-Functionalized *Si-Ox*^{Echem} and *Si-Ox*^{Chem} Surfaces and Its Implication on the Kinetics of AuNPs Anchoring. A deeper understanding of the kinetics of AuNPs surface coverage of each substrate (APS-functionalized ***Si-Ox*^{Echem}** or ***Si-Ox*^{Chem}** surfaces), at both APTES concentrations, could only be obtained by a careful characterization of the surfaces before and after APTES functionalization. For such a purpose two characterization techniques were employed: XPS and AFM.

XPS is a highly sensitive diagnostic method for functionalized surfaces. Using this method, two relevant quantities for the present purposes could be obtained: the oxide thickness and the relative number of different functional groups present on each surface. The XPS measurements of ***Si-Ox*^{Echem}** and ***Si-Ox*^{Chem}** substrates before and after APS-functionalization are shown in Figure 5. Signals of different intensities corresponding to oxygen, nitrogen, carbon, and silicon can be observed in the

dx.doi.org/10.1021/jp212613f | J. Phys. Chem. C 2013, 117, 11317−11327

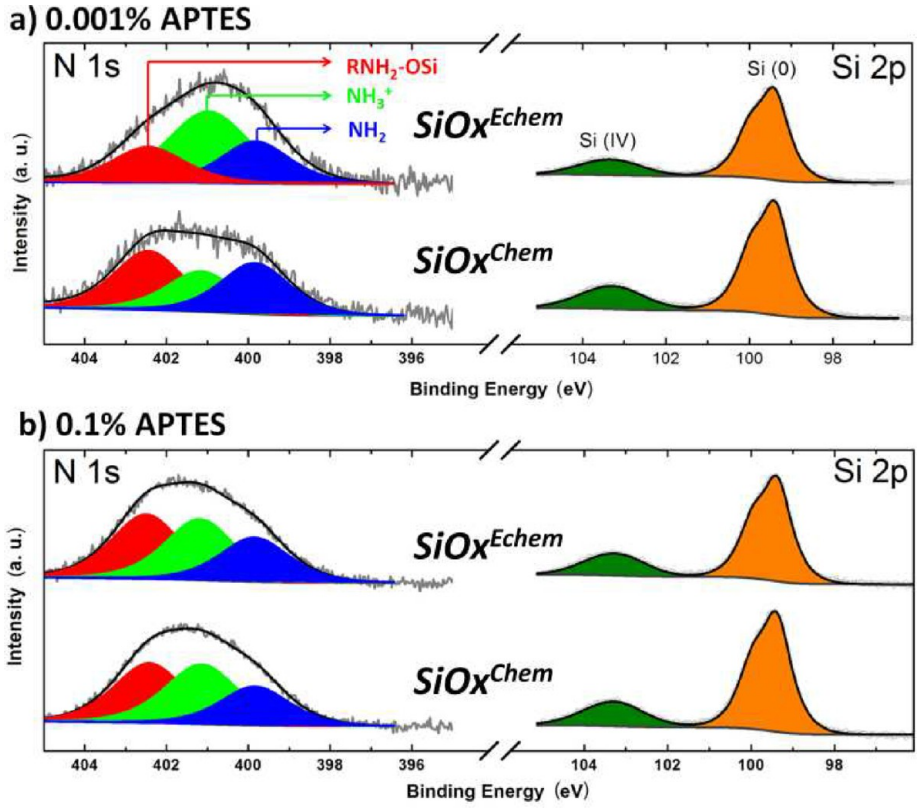

Figure 6. Deconvoluted XP spectra for N 1s and Si 2p signals after APS functionalization of ***Si-Ox***^{Echem} and ***Si-Ox***^{Chem} surfaces, with 0.001% (a) or 0.1% (b) APTES.

XP spectra, depending on the different surface treatments. The signal from N 1s (~401 eV) detected on both surfaces allows us to account qualitatively for the presence of an APS layer on the surfaces. In addition, the signal from C 1s (~286 eV) also supports this evidence because its intensity increases with APTES concentration; however, the presence of C 1s peak was also detected (weak signal) on both oxidized surfaces, possibly resulting from organic contamination (Figure 5a,a′).

XP spectra of the Si 2p signals corresponding to the ***Si-Ox***^{Echem} and ***Si-Ox***^{Chem} samples before APS functionalization are shown in Figure S5 in the Supporting Information. The Si 2p signals have two main components that peak at around 100 and 103.5 eV, attributed to the bulk silicon Si(0) and to the silane and oxide Si(IV), respectively. From the area's ratio between Si(IV) and Si(0) contributions of the Si 2p signals, the thickness of the oxide layers was determined.[39,40] The values of thickness for both oxide layers were found to be very small, around 1.1 and 1.2 nm for the ***Si-Ox***^{Echem} and ***Si-Ox***^{Chem} samples, respectively (Table 2). Although the thickness of both thin oxide films was found to be approximately the same, as it will be discussed later, the AFM measurements demonstrate that there are noticeable differences on the surface roughness between ***Si-Ox***^{Echem} and ***Si-Ox***^{Chem} samples.

After APS functionalization, the high binding energy side of the N 1s core level shows a complex structure, and the signal can be deconvoluted into three peaks at 399.9, 401.0, and 402.5 eV, assigned to free amines $-NH_2$ (blue area), protonated amines $-NH_3^+$ (green area), and amino groups interacting with hydroxil groups or directly with other silicon atoms RNH_2-OSi (red area), respectively, as depicted in Figure 6.[41,42] The presence of the last group is clear evidence that there is some degree of polymerization in all of the APS films.[42] It is worthwhile to remark on the quite different XP spectra profile for N 1s of the ***Si-Ox***^{Echem} functionalized at the lowest APTES concentration compared with the other three spectra profiles.

Table 2 shows explicitly the percentage contents of the different amino groups ($-NH_2$, $-NH_3^+$, and RNH_2-OSi) relative to the silicon atoms in the bulk for the APS layers formed at the two APTES concentrations employed to functionalize the ***Si-Ox***^{Echem} and ***Si-Ox***^{Chem} surfaces. The first feature to be noticed is that in the APS layer obtained with 0.1% APTES the relative percentage content of every type of amino group is almost the same (within the experimental error) for both substrates. In addition, because of the almost equal relative number of RNH_2-OSi groups for the ***Si-Ox***^{Echem} and ***Si-Ox***^{Chem} samples, in view of the discussion above, the degree of polymerization of the APS layer should also be the same. The anchoring sites of the AuNPs should be mainly the $-NH_3^+$ groups on the APS film because the negative charge of the citrate-capped AuNPs should favor the interaction with the positive-charged $-NH_3^+$ groups. Therefore, it is expected that both surfaces should have the same probability to anchor AuNPs. These results are in agreement with the almost identical kinetics parameters obtained for both surfaces at the highest APTES concentration.

In contrast, at the lowest APTES concentration there are significant differences in the relative number of $-NH_3^+$ and RNH_2-OSi moieties for the ***Si-Ox***^{Echem} and ***Si-Ox***^{Chem} samples in the respective APS layers. In this case, for the APS layer formed on the ***Si-Ox***^{Echem} surface the contribution assigned to RNH_2-OSi moieties is the lowest and that of $-NH_3^+$ groups is the highest (see Figure 6 and Table 2). Therefore, it should necessarily be inferred that again the availability of $-NH_3^+$ is what actually controls the kinetics of the AuNPs anchoring

dx.doi.org/10.1021/jp212613f | J. Phys. Chem. C 2013, 117, 11317−11327

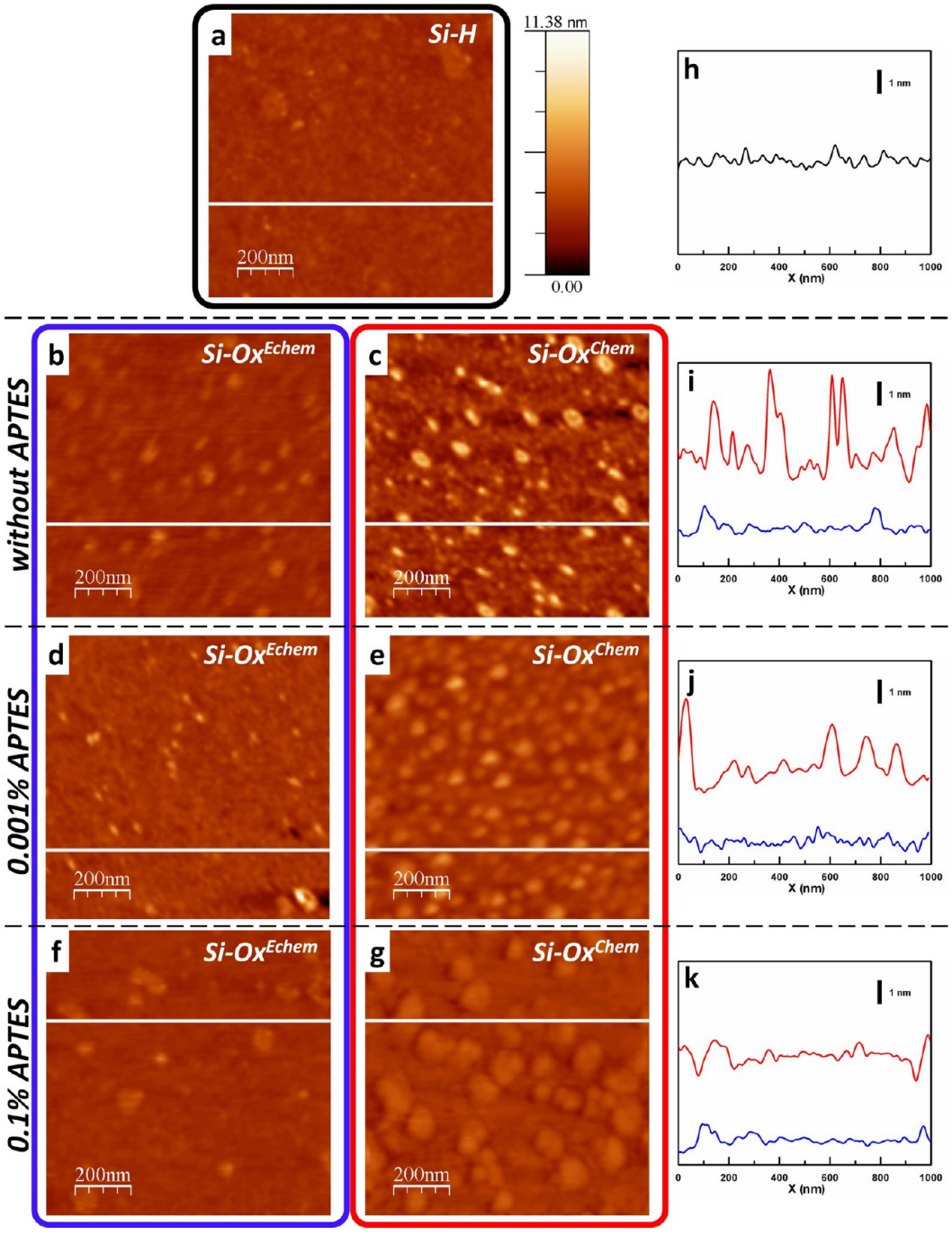

Figure 7. 1 μm × 1 μm AFM images of ***Si-H*** (a) and ***Si-Ox***^{Echem} and ***Si-Ox***^{Chem} before and after APTES functionalization (b–g) and respective topographic profiles (h–k) of ***Si-H*** (black line), ***Si-Ox***^{Echem} (blue lines), and ***Si-Ox***^{Chem} (red lines) surfaces, which were chosen as representative of the rms values given in Table 3.

process, as this quantity is almost 2.6 times greater in the ***Si-Ox***^{Echem} surface (1.8%) than in the ***Si-Ox***^{Chem} sample (0.7%). This result is in excellent agreement with the fact that the initial rate for AuNPs anchoring is around three times greater for the ***Si-Ox***^{Echem} than for the ***Si-Ox***^{Chem} surface. (See Table 2.)

Note that it is also observed that the relative total amount of N 1s is not the same for all functionalized surfaces; therefore, it should be instructive to compare the results by normalizing each relative percentage (corresponding to each amino species) with respect to the relative total amount of N 1s, as indicated in parentheses in Table 2. The conclusions outlined above are not changed at all using these values, rather they constitutes a further support to them. Using these data, one now realizes that at the lowest APTES concentration almost half of the N-containing groups are in the form $-NH_3^+$ in the electrochemically treated surface, while in the chemical one, almost a quarter is in this form. It is clear that the ***Si-Ox***^{Echem} surface functionalized with 0.001% APTES has the lowest normalized content of RNH_2-OSi, which is also indicative that this surface presents the lowest degree of APS polymerization (Table 2, figures in parentheses).

It is also clear that the almost identical kinetics behavior of the ***Si-Ox***^{Echem} surfaces at the lowest and the highest APTES concentrations is due to the fact that both surfaces have the

dx.doi.org/10.1021/jp212613f | J. Phys. Chem. C 2013, 117, 11317–11327

same availability of $-NH_3^+$ groups, while the ***Si-Ox***^{Chem} surfaces have significant differences in the number of $-NH_3^+$ groups that are responsible of the quite different kinetics at both APTES concentrations.

Now the question that arises is why at two quite different APTES concentrations do the ***Si-Ox***^{Echem} surfaces have the same number of $-NH_3^+$ groups and therefore the same kinetics, while in the ***Si-Ox***^{Chem} surfaces the availability of $-NH_3^+$ groups is very different, giving rise to a quite different kinetics behavior. As it will be demonstrated below, the significant difference in the roughness between both surfaces is the key parameter that could give an explanation to this issue.

Characterization of surfaces by AFM allows us to compare the roughness and homogeneity of the samples. AFM images of ***Si-H***, ***Si-Ox***^{Echem}, and ***Si-Ox***^{Chem} surfaces before APS functionalization are shown in Figure 7a–c. To determine the average surface roughness, the rms values for each sample were calculated, taking into account all of the points in the scanned area on the surface of the corresponding AFM image. As it can be appreciated, the ***Si-Ox***^{Echem} is smooth and the roughness value on atomic scale (Table 3) can be evaluated by its rms

Table 3. Surface Roughness (rms) Data for *Si-H*, *Si-Ox*^{Echem}, and *Si-Ox*^{Chem} Surfaces before and After APTES Functionalization, Obtained from AFM Images in Figure 7[a]

	rms (nm)		
surface	without APTES	0.001% APTES	0.1% APTES
Si-H	0.2		
Si-Ox^{Echem}	0.3	0.3	0.3
Si-Ox^{Chem}	1.0	0.6	0.4

[a]rms values were calculated by using all of the image data.

value = 0.3 nm, which is similar to the hydrogenated surface.[43,44] Quite remarkable, the ***Si-Ox***^{Chem} substrate has the highest rms value = 1.0 nm, being by far the most rough surface. Comparative profiles on the *z* axis of the topography each surface (depicted in Figure 7h,i) clearly highlight the features mentioned above for the ***Si-H***, ***Si-Ox***^{Echem}, and ***Si-Ox***^{Chem}. Note that each *z*-axis profile shown in Figure 7 was chosen in such a way as to be representative of the measured rms value. Given the differences of the surface roughness between both oxidized samples, one can argue that the ***Si-Ox***^{Chem} surface should have more deep valleys and cavities.

After functionalization with 0.1% APTES solution, both ***Si-Ox***^{Echem} and ***Si-Ox***^{Chem} films have almost the same surface roughness (slightly higher for the ***Si-Ox***^{Chem}). The surface topography after APS layer formation with 0.001% APTES is quite different depending on the preparation method, with the roughness greater for the APS films formed on ***Si-Ox***^{Chem} surfaces. (See Table 2 and Figure 7d–g,j,k.) The surface roughness of ***Si-Ox***^{Echem} samples does not change after functionalization with either 0.001 or 0.1% APTES concentration. In contrast, the rms values in the ***Si-Ox***^{Chem} surface change abruptly (from 1.0 to 0.6 nm and from 1.0 to 0.4 nm) by the formation of the APS layers at the lowest and highest APTES concentrations, respectively. It is reasonable to think that the smoothness of the surfaces is due to the preferential accumulation of molecules inside the above-mentioned cavities and valleys. This fact promotes APS polymerization inside the cavities; therefore, the relative content of the RNH_2-OSi groups changes from 1.1 to 2.5 by increasing the APTES concentration for the ***Si-Ox***^{Chem} surface functionalization (Table 2). Furthermore, the content of $-NH_3^+$ groups in the ***Si-Ox***^{Chem} functionalized surface is considerably higher when the APTES concentration is increased, in agreement with the kinetics behavior shown in Figure 4. This means that for a very rough surface such as the ***Si-Ox***^{Chem} sample the APTES concentration plays a significant role in the availability of $-NH_3^+$ groups. This is because APS polymerization inside the cavities on the surface decreases the relative number of $-NH_3^+$ groups; however, if the APS layer has a greater total content of nitrogen, the roughness is not important since once the cavities are almost completely filled with APS, a further functionalization process proceeds in the same way as a relative smooth surface. The above arguments explain why the ***Si-Ox***^{Chem} and ***Si-Ox***^{Echem} surfaces have almost the same number of active sites for anchoring Au nanoparticles after functionalization with 0.1% APTES. In contrast, this amount is quite different at the lowest APTES concentration.

A pictorial description of the changes of the silicon surface in the different stages of the surface modification is shown in Scheme 1. The surface treatment includes the following steps: oxidation, functionalization with APTES molecules, and AuNPs immobilization. Oxidation of the ***Si-H*** surfaces is performed either by electrochemical oxidation in aqueous solutions (***Si-Ox***^{Echem} surfaces) or by chemical oxidation in piranha solution

Scheme 1. Summary of the Different Stages of *Si-H* Surface Treatments: Oxidation (Electrochemical and Chemical Methods), Functionalization with APTES, and AuNPs Immobilization[a]

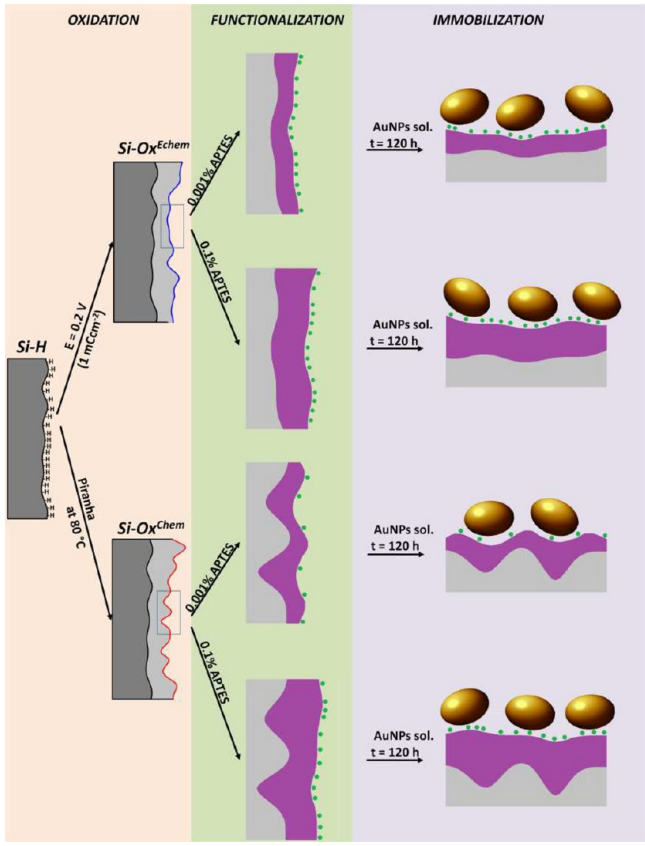

[a]Distribution of $-NH_3^+$ groups of the APS layers is highlighted for each APTES concentration (green circles) according to the information provided by XPS and AFM data.

(*Si-Ox*^{Chem} surfaces). The main difference between both treatments is associated with the surface roughness. Both types of oxidized surfaces are functionalized with APTES molecules. Depending on the APTES concentration, the availability of $-NH_3^+$ or reactive sites is different. During the AuNPs immobilization, σ values are independent of the oxidation treatment of the samples when the functionalization is performed with concentrated APTES solutions, whereas for the lowest APTES concentration, the *Si-Ox*^{Echem} surfaces present more $-NH_3^+$ sites for NPs immobilization than the *Si-Ox*^{Chem} surface.

4. CONCLUSIONS

In this work, we have demonstrated that the kinetics of AuNPs anchoring on APS-functionalized *Si-Ox* surfaces is a complex process because it depends on the chemical or electrochemical method of silicon surface oxidation, as well as on the APTES concentration used for APS modification.

At the highest APTES concentration, the kinetics of the AuNPs surface coverage is almost independent of how the oxidation of the surface (chemical or electrochemical) is performed. In contrast, at the lowest APTES concentration, the kinetics of AuNPs surface coverage is highly dependent on the oxidation method. Combining AFM and XPS measurements we were able to explain the different kinetics in terms of the availability of $-NH_3^+$ receptor sites in the APS layer. Quite remarkable, we discovered that there is close relationship between surface roughness and the number of reactive sites for anchoring AuNPs, mainly at the lowest APTES concentration. Chemical oxidation of the silicon gives rise to very rough surfaces that would favor the formation of RNH_2-OSi groups over the $-NH_3^+$ moieties, as shown by the XPS analysis. Once, after functionalization, either the *Si-Ox*^{Chem} or the *Si-Ox*^{Echem} surfaces have reached the same roughness (~0.3 nm), the probability of formation of RNH_2-OSi moieties is almost equal as well as the availability of $-NH_3^+$ groups. These features explain the similar kinetics behavior of the *Si-Ox*^{Chem} and *Si-Ox*^{EChem} surfaces at the highest APTES concentration, which is also equal to the kinetics behavior of the *Si-Ox*^{Echem} at the lowest APTES concentration. The *Si-Ox*^{Chem} surface at the lowest APTES concentration gives rise to an APS film with a considerable rms value (0.6 nm) but lower than the rms (1.0 nm) of the initial *Si-Ox*^{Chem} surface, indicating that the APS molecules fill the cavities but at the same time this filling is not enough to level off the whole surface. As a consequence, the degree of APS polymerization in the *Si-Ox*^{Chem} surface is greater than the number of $-NH_3^+$ groups, being by far the surface with the lowest number of active sites for anchoring Au nanoparticles. These results explain the low initial kinetics rate for anchoring AuNPs and also the smallest asymptotic percentage of AuNP surface coverage.

Although the present XPS results did not allow us to discriminate if a NP is bonded to one, two, or even more NH_3^+ groups, nor were we able to have a map of the distribution of these groups on the outmost surface (for this purpose, metastable induced electron spectroscopy (MIES) measurements should be very suitable),[18] we have shown how by combining SEM, AFM, and XPS analysis we were able to explain the complex kinetics of AuNPs anchoring process on the different *Si-Ox* surface-functionalized surfaces based on the total number of NH_3^+ groups, which we have demonstrated is determined mainly by the interplay between surface roughness and APTES concentration.

■ ASSOCIATED CONTENT

Supporting Information

TEM and optical characterization of gold nanoparticles synthetized by the Turkevich method. SEM images of a *Si-Ox*^{Echem} sample. XP spectra of Si 2p region from both *Si-Ox*^{Echem} and *Si-Ox*^{Echem}. This material is available free of charge via the Internet at http://pubs.acs.org.

■ AUTHOR INFORMATION

Corresponding Author

*E-mail: glacconi@fcq.unc.edu.ar (G.I.L.); coronado@fcq.unc.edu.ar (E.A.C.). Phone: +54-351-4334169. Fax: +54-351-4334188.

Notes

The authors declare no competing financial interest.

■ ACKNOWLEDGMENTS

J.K. and L.A.P. have contributed equally to this manuscript. We thank CONICET, FONCyT, LAMARX FAMAF-UNC, PME (2006) 1544, and SECyT-UNC for financial support. J.K. and L.A.P. also thank CONICET and FONCyT/SECyT PFDT, respectively, for the fellowships granted. We also thank G. Benitez for XPS measurements in INIFTA-UNLP and D. Brusa and C. Schürrer for AFM analysis in CEMETRO UTN-FRC.

■ REFERENCES

(1) Xia, Y.; Ramgopal, Y.; Li, H.; Shang, L.; Srinivas, P.; Kickhoefer, V. A.; Rome, L. H.; Preiser, P. R.; Boey, F.; Zhang, H.; Venkatraman, S. S. Immobilization of Recombinant Vault Nanoparticles on Solid Substrates. *ACS Nano* **2010**, *4*, 1417−1424.

(2) Kannan, P.; John, S. A. Highly Sensitive Electrochemical Determination of Nitric Oxide Using Fused Spherical Gold Nanoparticles Modified ITO electrode. *Electrochim. Acta* **2010**, *55*, 3497−3503.

(3) Kajiura, M.; Nakanishi, T.; Iida, H.; Takada, H.; Osaka, T. Biosensing by Optical Waveguide Spectroscopy Based on Localized Surface Plasmon Resonance of Gold Nanoparticles Used as a Probe or as a Label. *J. Colloid Interface Sci.* **2009**, *335*, 140−145.

(4) Spadavecchia, J.; Prete, P.; Lovergine, N.; Tapfer, L.; Rella, R. Au Nanoparticles Prepared by Physical Method on Si and Sapphire Substrates for Biosensor Applications. *J. Phys. Chem. B* **2005**, *109*, 17347−17349.

(5) Touahir, L.; Allongue, P.; Aureau, D.; Boukherroub, R.; Chazalviel, J.-N.; Galopin, E.; Gouget-Laemmel, A. C.; Henry de Villeneuve, C.; Moraillon, A.; Niedziółka-Jőnsson, J.; Ozanam, F.; Salvador Andresa, J.; martSam, S.; Solomon, I.; Szunerits, S. Molecular Monolayers on Silicon as Substrates for Biosensors. *Bioelectrochemistry* **2010**, *80*, 17−25.

(6) Su, Q.; Ma, X.; Dong, J.; Jiang, C.; Qian, W. A Reproducible SERS Substrate Based on Electrostatically Assisted APTES-Functionalized Surface-Assembly of Gold Nanostars. *ACS Appl. Mater. Interfaces* **2011**, *3*, 1873−1879.

(7) Hashimoto, S.; Uwada, T.; Hagiri, M.; Shiraishi, R. Mechanistic Aspect of Surface Modification on Glass Substrates Assisted by Single Shot Pulsed Laser-Induced Fragmentation of Gold Nanoparticles. *J. Phys. Chem. C* **2011**, *115*, 4986−4993.

(8) Nath, N.; Chilkoti, A. Label-Free Biosensing by Surface Plasmon Resonance of Nanoparticles on Glass: Optimization of Nanoparticle Size. *Anal. Chem.* **2004**, *76*, 5370−5378.

(9) Gerber, R. W.; Leonard, D. N.; Franzen, S. Conductive Thin Film Multilayers of Gold on Glass Formed by Self-Assembly of Multiple Size Gold Nanoparticles. *Thin Solid Films* **2009**, *517*, 6803−6808.

(10) Zhang, Z.; Wu, Y. Investigation of the NaBH4-Induced Aggregation of Au Nanoparticles. *Langmuir* **2010**, *26*, 9214−9223.

(11) Smith, E. A.; Chen, W. How to Prevent the Loss of Surface Functionality Derived from Aminosilanes. *Langmuir* **2008**, *24*, 12405−12409.
(12) Grabar, K. C.; Allison, K. J.; Baker, B. E.; Bright, R. M.; Brown, K. R.; Griffith Freeman, R.; Fox, A. P.; Keating, C. D.; Musick, M. D.; Natan, M. J. Two-Dimensional Arrays of Colloidal Gold Particles: A Flexible Approach to Macroscopic Metal Surfaces. *Langmuir* **1996**, *12*, 2353−2361.
(13) Thissen, P.; Peixoto, T.; Longo, R. C.; Cho, K.; Schmidt, W. G.; Chabal, Y. J. Activation of Surface Hydroxyl Groups by Modification of H-Terminated Si(111) Surfaces. *J. Am. Chem. Soc.* **2012**, *134*, 8869−8874.
(14) Aureau, D.; Varin, Y.; Roodenko, K.; Seitz, O.; Pluchery, O.; Chabal, Y. J. Controlled Deposition of Gold Nanoparticles on Well-Defined Organic Monolayer Grafted on Silicon Surfaces. *J. Phys. Chem. C* **2010**, *114*, 14180−14186.
(15) Harnisch, J. A.; Pris, A. D.; Porter, M. D. Attachment of Gold Nanoparticles to Glassy Carbon Electrodes via a Mercaptobenzene Film. *J. Am. Chem. Soc.* **2001**, *123*, 5829−5830.
(16) Shirman, T.; Kaminker, R.; Freeman, D.; Van der Boom, M. E. Halogen-Bonding Mediated Stepwise Assembly of Gold Nanoparticles Onto Planar Surfaces. *ACS Nano* **2011**, *5*, 6553−6563.
(17) Zhang, Z.; Wu, Y. $NaBH_4$-Induced Assembly of Immobilized Au Nanoparticles into Chainlike Structures on a Chemically Modified Glass Surface. *Langmuir* **2011**, *27*, 9834−9842.
(18) Acres, R. G.; Ellis, A. V.; Alvino, J.; Lenahan, C. E.; Khodakov, D. A.; Metha, G. F.; Andersson, G. G. Molecular Structure of 3-Aminopropyltriethoxysilane Layers Formed on Silanol-Terminated Silicon Surfaces. *J. Phys. Chem. C* **2012**, *116*, 6289−6297.
(19) Scarpettini, A. F.; Bragas, A. V. Coverage and Aggregation of Gold Nanoparticles on Silanized Glasses. *Langmuir* **2010**, *26*, 15948−15953.
(20) Kim, J.; Dantelle, G.; Revaux, A.; Bérard, M.; Huignard, A.; Gacoin, T.; Boilot, J. P. Plasmon-Induced Modification of Fluorescent Thin Film Emission Nearby Gold Nanoparticle Monolayers. *Langmuir* **2010**, *26*, 8842−8849.
(21) Li, H.; Zhang, J.; Zhou, X.; Lu, G.; Yin, Z.; Li, G.; Wu, T.; Boey, F.; Benkatraman, S. S.; Zhang, H. Aminosilane Micropatterns on Hydroxyl-Terminated Substrates: Fabrication and Applications. *Langmuir* **2010**, *26*, 5603−5609.
(22) Praig, V. G.; Piret, G.; Manesse, M.; Castel, X.; Boukherroub, R.; Szunerits, S. Seed-Mediated Electrochemical Growth of Gold Nanostructures on Indium Tin Oxide Thin Films. *Electrochim. Acta* **2008**, *53*, 7838−7844.
(23) Kosuda, K. M.; Bingham, J. M.; Wustholz, K. L.; Van Duyne, R. P. In *Comprehensive Nanoscience and Technology*; Andrews, D. L., Scholes, G. D., Wiederrecht, G. P., Eds.; Academic Press: Oxford, U.K., 2011; Vol. 3, pp 263−301.
(24) Zheng, J.; Zhu, Z.; Chen, H.; Liu, Z. Nanopatterned Assembling of Colloidal Gold Nanoparticles on Silicon. *Langmuir* **2000**, *16*, 4409−4412.
(25) Böhmler, J.; Ploux, L.; Ball, V.; Anselme, K.; Ponche, A. Necessity of a Thorough Characterization of Functionalized Silicon Wafers before Biointerface Studies. *J. Phys. Chem. C* **2011**, *115*, 11102−11111.
(26) Pasternack, R. M.; Rivillon Amy, S.; Chabal, Y. J. Attachment of 3-(Aminopropyl)triethoxysilane on Silicon Oxide Surfaces: Dependence on Solution Temperature. *Langmuir* **2008**, *24*, 12963−2971.
(27) Kallury, K. M. R.; Macdonald, P. M.; Thompson, M. Effect of Surface Water and Base Catalysis on the Silanization of Silica by (Aminopropyl)alkoxysilanes Studied by X-ray Photoelectron Spectroscopy and 13C Cross-Polarization/Magic Angle Spinning Nuclear Magnetic Resonance. *Langmuir* **1994**, *10*, 492−499.
(28) Lapin, N. A.; Chabal, Y. J. Infrared Characterization of Biotinylated Silicon Oxide Surfaces, Surface Stability, and Specific Attachment of Streptavidin. *J. Phys. Chem. B* **2009**, *113*, 8776−8783.
(29) Seitz, O.; Fernandez, P. G.; Tian, R.; Karnik, N.; Wen, H.-C.; Stiegler, H.; Chapman, R. A.; Vogel, E. M.; Chabal, Y. J. Control and Stability of Self-Assembled Monolayers Under Biosensing Conditions. *J. Mater. Chem.* **2011**, *21*, 4384−4392.
(30) Horcas, I.; Fernandez, R.; Gomez-Rodriguez, J. M.; Colchero, J.; Gómez-Herrero, J.; Baro, A. M. WSXM: A Software for Scanning Probe Microscopy and a Tool for Nanotechnology. *Rev. Sci. Instrum.* **2007**, *78*, 013705.
(31) Bensliman, F.; Fukuda, A.; Mizuta, N.; Matsumura, M. Analysis of Anodic Oxidation Current of Flattened p-Type Si(111) Surface in Aqueous Solution. *J. Electrochem. Soc.* **2003**, *150*, G527−G531.
(32) Turkevich, J.; Stevenson, P. C.; Hillier, J. A Study of the Nucleation and Growth Processes in the Synthesis of Colloidal Gold. *Discuss. Faraday Soc.* **1951**, *11*, 55−75.
(33) John, S. A.; Sagara, T. Short-Time Preparation and Electrochemical Properties of a Single Layer of Tetraoctylammonium Bromide Capped Au Nanoparticles on Dithiol Self-Assembled Monolayer-Modified Au Electrode. *J. Electroanal. Chem.* **2009**, *633*, 175−181.
(34) Wayner, D. D. M.; Wolkow, R. A. Organic Modification of Hydrogen Terminated Silicon Surfaces. *J. Chem. Soc., Perkin Trans.* **2002**, *2*, 23−34.
(35) Vegunta, S. S. S.; Ngunjiri, J. N.; Flake, J. C. Electrochemical and Thermal Grafting of Alkyl Grignard Reagents onto (100) Silicon Surfaces. *Langmuir* **2009**, *25*, 12750−12756.
(36) Muñoz, A. G.; Moehring, A.; Lohrengel, M. M. Anodic Oxidation of Chemically Hydrogenated Si(100). *Electrochim. Acta* **2002**, *47*, 2751−2760.
(37) Li, H.; Perkas, N.; Li, Q.; Gofer, Y.; Koltypin, Y.; Gedanken, A. Improved Silanization Modification of a Silica Surface and Its Application to the Preparation of a Silica-Supported Polyoxometalate Catalyst. *Langmuir* **2003**, *19*, 10409−10413.
(38) Kim, J.; Seidler, P.; Wan, L. S.; Fill, C. Formation, Structure, and Reactivity of Amino-Terminated Organic Films on Silicon Substrates. *J. Colloid Interface Sci.* **2009**, *329*, 114−119.
(39) Gunter, P. L. J.; De Jong, A. M.; Niemantsverdriet, J. W.; Rheiter, H. J. H. Evaluation of Take-Off-Angle-Dependent XPS for Determining the Thickness of Passivation Layers on Aluminium and Silicon. *Surf. Interface Anal.* **1992**, *19*, 161−164.
(40) Tanuma, S.; Powell, C. J.; Penn, D. R. Calculations of Electrn Inelastic Mean Free Paths for 31 Materials. *Surf. Interface Anal.* **1988**, *11*, 577−589.
(41) Mäkila, E.; Bimbo, L. M.; Kaasalainen, M.; Herranz, B.; Airaksinen, A. J.; Heinonen, M.; Kukk, E.; Hirvonen, J.; Santos, H. A.; Salonen, J. Amine Modification of Thermally Carbonized Porous Silicon with Silane Coupling Chemistry. *Langmuir* **2012**, *28*, 14045−14054.
(42) Hong, J.; Zaera, F. Interference of the Surface of the Solid on the Performance of Tethered Molecular Catalysts. *J. Am. Chem. Soc.* **2012**, *134*, 13056−13065.
(43) Munford, M. L. Electrodeposicao de Nanoestruturas Metalicas em Silicio Monocristalino, Ph. D. Thesis, Universidade Federal de Santa Catarina, Brazil, 2002.
(44) Higashi, H. S.; Chabal, Y. J. In *Handbook of Semiconductor Wafer Cleaning Technology*; Kern, W., Ed.; Noyes Publications: Park Ridge, NJ, 1993; p 433.